JOURNAL OF SOLID STATE CHEMISTRY **124,** 353–359 (1996)
ARTICLE NO. 0249

Vibrational Spectroscopy and X-Ray Diffraction of Perovskite Compounds $Sr_{1-x}M_xTiO_3$ (M = Ca, Mg; $0 \leq x \leq 1$)

T. Hirata,[1] K. Ishioka, and M. Kitajima

National Research Institute for Metals, 1-2-1, Sengen, Tsukuba, Ibaraki 305, Japan

Received December 11, 1995; in revised form April 12, 1996; accepted April 22, 1996

A series of perovskite compounds, $Sr_{1-x}M_xTiO_3$ (M = Ca, Mg; $0 \leq x \leq 1$), has been synthesized by solid-state reaction, and characterized by Fourier-transform infrared spectroscopy, Raman scattering, and X-ray diffraction. As for $Sr_{1-x}Ca_xTiO_3$, it was found that the substitutional solid solutions are formed over a wide x range, whereas traces of orthorhombic $CaTiO_3$ would appear for $x \geq 0.6$. The unit-cell volume of cubic $SrTiO_3$ decreases as Sr is replaced by Ca with a smaller ionic radius, and the Sr–O bond length reduction is somewhat matched by the Ti–O bond shortening. The latter is evidenced by the fact that the 460 cm^{-1} Raman band assigned to the Ti–O_3 torsional mode appears at $x = 0.6$ and shifts upward with further increasing x. On the other hand, the formation of solid solutions is restricted to $x \leq 0.2$ for $Sr_{1-x}Mg_xTiO_3$; the Raman/infrared-reflectivity spectra and X-ray diffraction profiles of $Sr_{1-x}Mg_xTiO_3$ are characteristic of the coexistence of cubic $SrTiO_3$ and hexagonal $MgTiO_3$. The solubility of Ca or Mg in $SrTiO_3$ is discussed based on the correlation between the enthalpy and tolerance factors for $A^{II}B^{IV}O_3$. It is concluded that inefficient mixing of $MgTiO_3$ with $SrTiO_3$ is predominated by the substantial difference between the Sr^{2+} and Mg^{2+} cation radii; this accounts for the less stable $Sr_{1-x}Mg_xTiO_3$ and the more limited solubility of Mg in $SrTiO_3$ as well, through the effective difference in the tolerance factors of $SrTiO_3$ and $MgTiO_3$ as compared with $CaTiO_3$.

1. INTRODUCTION

The perovskite compound $SrTiO_3$ undergoes the cubic (O_h^1; $Pm3m$) to tetragonal (D_{4h}; $4/mmm$) phase transition at ~105 K (1). This phase transition and its effect on the OH stretching mode have been studied in $SrTiO_3$ and its related compounds (2–5). Advantageously, the perovskite compounds of the general formula ABO_3 are tailored to modification of crystallographic, electronic, and physical properties by replacing the A or B cations by other A' or B' cations with different radius/charge forming $A_{1-x}A'_xBO_3$ or $AB_{1-y}B'_yO_3$ (6), while this end is also achieved by stoichiometry control with respect to oxygen. It is taken for granted that the single uniform phase of $A_{1-x}A'_xBO_3$ or $AB_{1-y}B'_yO_3$ is formed over a wide composition range when the A or B cations are replaced by other A' or B' cations with the same charge and similar ionic radius, as demonstrated by successful synthesis of a continuous series of the solid solutions $SrTi_{1-y}Ru_yO_3$ (7). However, the structural change of perovskite compounds can be induced upon cation substitution with different radius and the same or different charge.

The stability of the perovskite compounds is predicted by the so-called tolerance factor defined as $t = (r_A + r_O)[\sqrt{2}(r_B + r_O)]^{-1}$, where r_A and r_B are the average ionic radii at the A or B sites, respectively, and r_O is the ion radius of oxygen (8); the perovskite compounds ABO_3 are stabilized for $0.75 < t < 0.95$, and the ideal cubic structure of ABO_3 is substantiated for $t = 1$. The substitution of the A' or B' cations at the A or B sites in ABO_3 corresponds to altering the A–O and/or B–O bond distances, so that this bond mismatch causes a resultant change in t.

The perovskite compounds $Nd_{1-x}A_xTiO_3$ (A = Ca, Sr, Ba; $0 \leq x \leq 1$) (9, 10) and $Ce_{1-x}A_xTiO_3$ (A = Sr, Ba; $0 \leq x \leq 0.8$) (11) have been synthesized, and their structural, transport, electronic, and magnetic properties were investigated in detail. Using the effective ion radii of Shannon (12), it turns out that the t's of all these perovskite compounds increase with x. This urges us to study any perovskite compounds whose tolerance factors decrease upon substitution. To this end, in the present work, the two systems $Sr_{1-x}Ca_xTiO_3$ and $Sr_{1-x}Mg_xTiO_3$ were adopted; Ca and Mg have the same charge (2+) as Sr^{2+} but different ionic radii (rCa^{2+} = 1.34 Å and rMg^{2+} = 1.03 Å as compared with rSr^{2+} = 1.44 Å) (12). For the $SrTiO_3$–$CaTiO_3$ system, it has been found that the X-ray diffraction lines characteristic of orthorhombic $CaTiO_3$ are gradually transformed into the lines corresponding to cubic $SrTiO_3$, and that only displaced diffraction lines of $SrTiO_3$ are present at ~60 mol% $SrTiO_3$ (13); thus, the $SrTiO_3$–$CaTiO_3$ system forms the $Sr_{1-x}Ca_xTiO_3$ solid solutions over a wide x range. On the other hand, the $SrTiO_3$–$MgTiO_3$ system has not

[1] To whom correspondence should be addressed.

0022-4596/96 $18.00

been investigated in detail, while it is remarked in (14) that Mg is insoluble into $SrTiO_3$ because the structural packing density is different between $SrTiO_3$ (perovskite) and $MgTiO_3$ (ilmenite). There is a point in studying these two systems in view of that small amounts of $CaTiO_3$, $BaTiO_3$, and $MgTiO_3$ are usually added to $SrTiO_3$ for controlling its dielectric properties.

In addition, the metal–oxygen bond distances and bond angles are two important structural parameters which are relevant to the stability of the perovskite compounds. While the infrared and Raman spectra of $SrTiO_3$, $CaTiO_3$, and $MgTiO_3$ have been measured (2–5, 15–17), the substitution of other cations at the A and/or B sites alters the vibrational properties of ABO_3 studied by these spectroscopic techniques. This encourages us to measure the infrared and Raman spectra of $Sr_{1-x}M_xTiO_3$ (M = Ca, Mg), which contain information about the metal–oxygen stretching/bending vibrations and their x dependence as well.

2. EXPERIMENTAL

The series of perovskite compounds $Sr_{1-x}M_xTiO_3$ (M = Ca, Mg; $0 \le x \le 1$) was synthesized by solid-state reaction, starting with $SrTiO_3$, $CaTiO_3$, and $MgTiO_3$ powders (99.9%). These powders were weighed out so as to give $Sr_{1-x}M_xTiO_3$ (M = Ca, Mg) with intervals of $x = 0.1$, and were intimately mixed in a mortar. Subsequently, the mixture was subjected to CIP (Cold Isostatic Pressing) at 1500 kgf/cm^2, and fired at 1100°C for 5 h several times to ensure its homogenization. Final sintering was performed in air at 1250°C for 18 h. The sintering in air assures $\delta = 0$ for $Sr_{1-x}M_xTiO_{3+\delta}$ (M = Ca, Mg), because the oxygen stoichiometry is variable over a considerable range in heat treatments under reducing atmosphere. From the sintered products, pellets (1 mm in thickness and 10 mm ϕ in diameter) were prepared for X-ray diffraction (XRD), infrared spectroscopy, and Raman scattering.

XRD was performed by an X-ray diffractometer (Rigaku Rintz500) with Cu$K\alpha$. Lattice parameters were refined by a least-squares fitting to the observed X-ray data between $2\theta = 20°$ and 90°. Infrared-reflectivity spectra were recorded by a Fourier-transform infrared spectrometer (JEOR JIR100) in two different wavenumber regions, 50–550 cm^{-1} and 400–4000 cm^{-1}; the resolution was 2 cm^{-1} in the far infrared and 4 cm^{-1} in the mid-infrared. Either beam splitter KBr or myler was used in each wavenumber region, along with a detector of TGS (tryglicine sulfate). A mirror of aluminium evaporated thin film was used as the reference, in order to express the infrared-reflectivity spectra as the sample to reference intensity ratio. Raman spectra were measured by a laser Raman spectrometer (JASCO TRS660) with a spectrometric multichannel analyzer (Princeton Inc. DRS700); the 514.5 nm Ar^+ laser was used as an exciting source with approximately 20 mW power, and all Raman spectra were recorded at room temperature in a backscattering geometry.

3. RESULTS

3.1. X-Ray Diffraction Profiles and Lattice Parameters

Figure 1a shows the XRD profiles of $Sr_{1-x}Ca_xTiO_3$ with different x's between $2\theta = 20°$ and 90°; the XRD profiles of the end members $SrTiO_3$ and $CaTiO_3$ are also shown, for reference. The XRD profiles of each end member can be indexed as cubic and orthorhombic unit cells, respectively; the lattice parameters were determined to be a = 3.908 Å for $SrTiO_3$ and a = 5.441 Å, b = 7.647 Å, and c = 5.379 Å for $CaTiO_3$, which are in agreement with the crystallographic data of each end member (7, 13). We notice that all Bragg reflections characteristic of $SrTiO_3$ shift upward with x. This is due to the lattice contraction as Sr is replaced by Ca with a smaller ionic radius in $Sr_{1-x}Ca_xTiO_3$. Besides, the (211) reflection of $CaTiO_3$ would appear at about $2\theta = 39°$ and persists for $x \ge 0.6$. No other major reflections due to $CaTiO_3$ appear except for this extra reflection. Consequently, it is regarded that the $Sr_{1-x}Ca_xTiO_3$ solid solutions are formed between $0 < x < 1$, but with traces of $CaTiO_3$ for $0.6 \le x \le 0.9$.

Figure 1b shows the XRD profiles of $Sr_{1-x}Mg_xTiO_3$ with different x's between $2\theta = 20°$ and 90°. The XRD profile of $MgTiO_3$ is indexed as a hexagonal unit cell with a = 5.058 Å and c = 13.910 Å, in agreement with the literature (18). It is evident that the XRD profiles of $Sr_{1-x}Mg_xTiO_3$ change systematically with x. The noticeable finding is that the reflections assigned to $MgTiO_3$ increase in intensity with x starting with $x \approx 0.3$, while all reflections due to $SrTiO_3$ decrease in intensity.

Figure 2 reveals the ''difference profile'' obtained by subtracting the XRD profile of $SrTiO_3$ from those of $Sr_{1-x}Mg_xTiO_3$ with $x \ge 0.1$ such that the (110) reflection due to $SrTiO_3$ is almost nil. This demonstrates the appearance of (110), (024), and (116) reflections due to $MgTiO_3$ at $x = 0.2$ and their evolution with x; this implies that the $Sr_{1-x}Mg_xTiO_3$ solid solutions are restricted to $x \le 0.2$. Note that some reflections other than the (110) reflection due to $SrTiO_3$ appear since each reflection shows its intensity variation depending on x's.

Figure 3a plots the lattice parameters of $Sr_{1-x}Ca_xTiO_3$ as a function of x; the unit-cell volume is shown as well. The lattice parameters of $Sr_{1-x}Ca_xTiO_3$ decrease with increasing x, causing a decrease in cell volume. The cubic unit cell of $SrTiO_3$ is transformed into the orthorhombic unit cell of $CaTiO_3$ by a transformation matrix (101, 020, -101), to compare with the previous results (13). Note that the result of Fig. 3a qualitatively agrees with (13), where the linear correlation between b, V, and x is demonstrated between $0 \le x \le 1$ in $Ca_{1-x}Sr_xTiO_3$; the data at

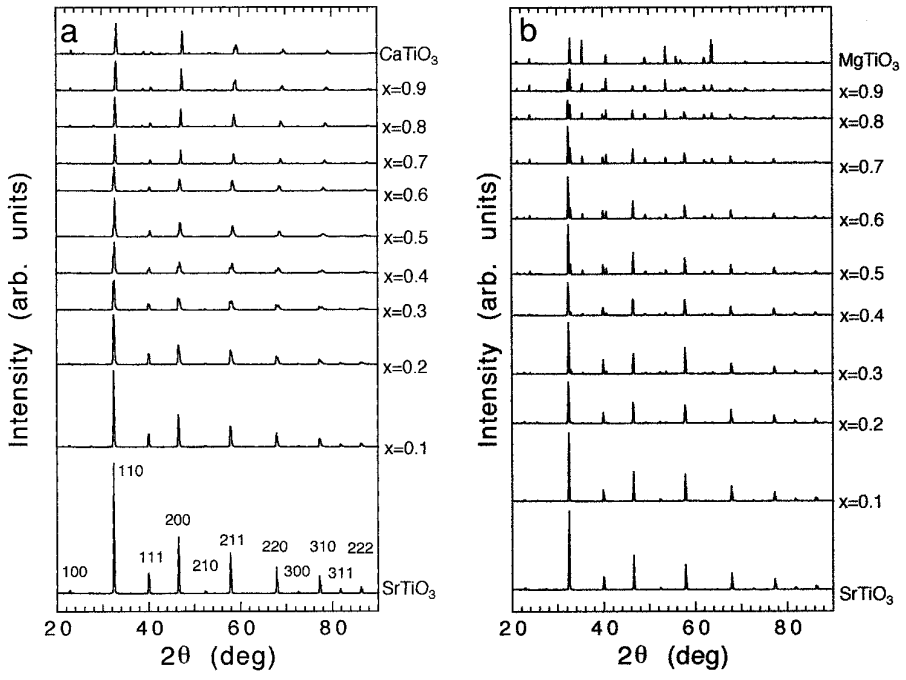

FIG. 1. The X-ray diffraction (XRD) profiles of $Sr_{1-x}Ca_xTiO_3$ (a) and $Sr_{1-x}Mg_xTiO_3$ (b) with different x's between $2\theta = 20°$ and 90°.

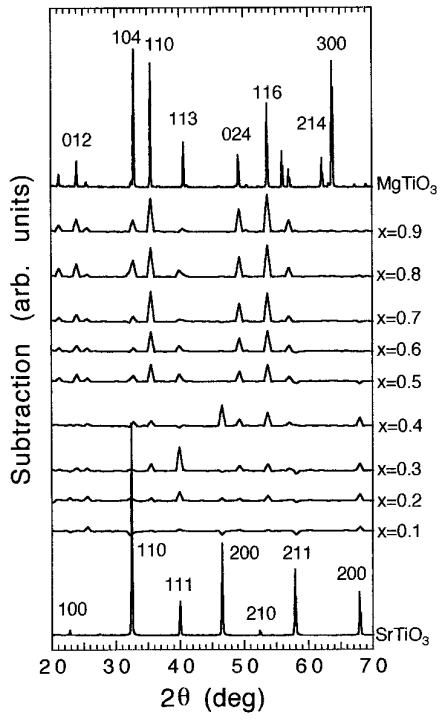

FIG. 2. The difference profile obtained by subtracting the XRD profile of $SrTiO_3$ from those of $Sr_{1-x}Mg_xTiO_3$ with $x \ge 0.1$ between $2\theta = 20°$ and 70°; the XRD profiles of $SrTiO_3$ and $MgTiO_3$ are also shown, for comparison.

$x = 0.2$–0.4 may account for the failure of the linear correlation in the present work.

Figure 3b plots the lattice parameters of $SrTiO_3$ and $MgTiO_3$ that are coexistent in $Sr_{1-x}Mg_xTiO_3$ as a function of x; the integrated intensities of the (110) and its neighboring (104) reflections due to $SrTiO_3$ and $MgTiO_3$ are shown as well. The lattice parameters of each phase remain unchanged with x, and the integrated intensity of the (110) reflection gradually decreases for $x \ge 0.2$ while the (104) reflection starts to increase in intensity from $x \approx 0.2$. This is further evidence for the inefficient mixing of $MgTiO_3$ with $SrTiO_3$.

3.2. Infrared-Reflectivity Spectra

Figure 4a shows the infrared-reflectivity spectra of $Sr_{1-x}Ca_xTiO_3$ between 50–550 cm^{-1} and 350–1000 cm^{-1}. The infrared-reflectivity spectra of $SrTiO_3$ and $CaTiO_3$ are shown, for comparison; the spectra of each end member are comparable to the literature (15, 19). The three infrared-active modes of symmetry F_{1u} are observed at 110, 190, and 565 cm^{-1} for cubic $SrTiO_3$ (C_h^1; $Pm3m$). The 565 cm^{-1} mode is characteristic of $SrTiO_3$, with a dip at 172 cm^{-1} between the two modes at 110 and 190 cm^{-1}. No band near 450 cm^{-1}, which was observed in the infrared-reflectivity spectrum of $SrTiO_3$ (20), is detected in the present work. On the other hand, the infrared-reflectivity spectra of orthorhombic $CaTiO_3$ (D_{2h}^{16}; $Pnma$) are characterized by the modes of symmetry B_1, B_2, and A_1 at 575, 455, 177, and 148 cm^{-1}. The two modes at 455 and 575

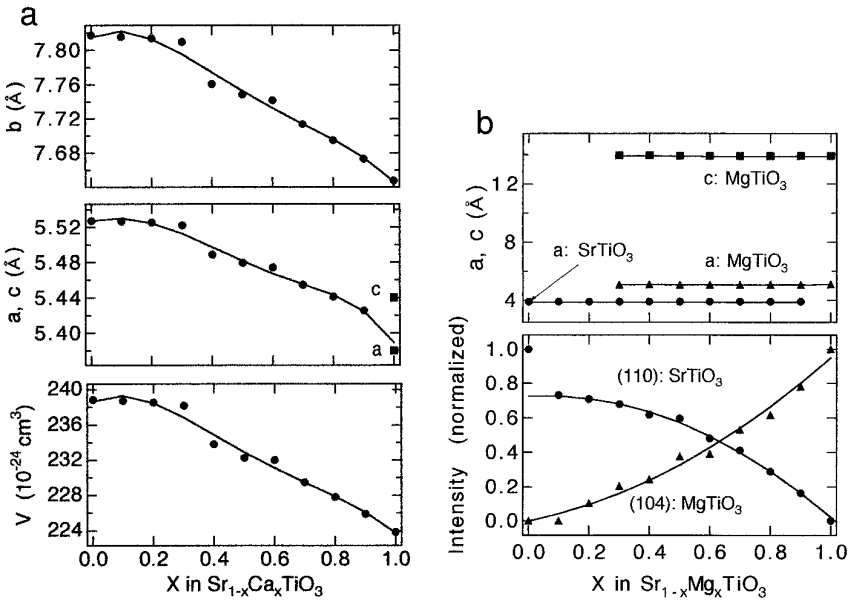

FIG. 3. The lattice parameters of $Sr_{1-x}Ca_xTiO_3$ (a) as a function of x; the unit-cell volume is shown as well. Note that the cubic unit cell of $SrTiO_3$ is transformed into the orthorhombic unit cell of $CaTiO_3$, to compare with the previous results (13). The lattice parameters of $SrTiO_3$ and $MgTiO_3$ that are coexistent in $Sr_{1-x}Mg_xTiO_3$ are shown in (b); the integrated intensities (normalized) of the (110) and (104) reflections due to $SrTiO_3$ and $MgTiO_3$ are also plotted as a function of x. The lines connecting the data points are only to guide the eye in (a) and (b).

cm^{-1} are representative of $CaTiO_3$. Meanwhile, we notice other spectral features—several dips in the far infrared spectrum of $CaTiO_3$. The infrared-active mode ν_1 at 565 cm^{-1} for $SrTiO_3$, assigned to the Ti–O stretch, shifts to the corresponding mode for $CaTiO_3$ at 575 cm^{-1} increasing its intensity with x; besides, the 455 cm^{-1} mode ν_2 for $CaTiO_3$ assigned to the Ti–O_3 torsion becomes pronounced with x evolving at $x \geq 0.6$. For modes at 177 and 148 cm^{-1}, which are assigned to the O–Ti–O bend and cation–TiO_3 lattice vibration, it seems hard to comment on their x dependence. The appearance of the two modes ν_1 and ν_2 at $x \geq 0.6$ assures traces of $CaTiO_3$ in $Sr_{1-x}Ca_xTiO_3$, as evidenced by the emerged (211) reflection due to $CaTiO_3$ in Fig. 1a.

Figure 4b indicates the infrared-reflectivity spectra of $Sr_{1-x}Mg_xTiO_3$ with different x's. The infrared-reflectivity spectrum of $MgTiO_3$ is in agreement with the literature (21), where the infrared-active modes of symmetry A_u or E_u are observed at 278, 321, 420, 472, 529, and 680 cm^{-1}, fewer than the infrared-active modes $4A_u$ and $4E_u$ predicted by the factor group analysis for $MgTiO_3$. Other infrared-active modes are resolved at 385 and 709–773 cm^{-1} as a shoulder and two humps, respectively, in the present spectrum of $MgTiO_3$. It should be recalled that 8 infrared modes are observed at 284, 350, 377, 420, 480, 550–620, 670, and 722 cm^{-1} in the infrared transmission spectra of $MgTiO_3$ (17). It seems that all these modes of $MgTiO_3$ would appear at $x \geq 0.3$ and increase in intensity with x in Fig. 4b. This observation is corroborated by the "difference spectrum" obtained by subtracting the infrared-reflectivity spectrum of $SrTiO_3$ from those of $Sr_{1-x}Mg_xTiO_3$ with $x \geq 0.1$, which could reproduce the two humps between 709–773 cm^{-1} and the distinct band around 550 cm^{-1} characteristic of $MgTiO_3$ for $x \geq 0.3$; consequently, it is concluded that the solubility of Mg in $SrTiO_3$ is limited to $x \leq 0.2$.

3.3. Raman Spectra

Figure 5a shows the Raman spectra of $Sr_{1-x}Ca_xTiO_3$ ($x = 0$–1) in the frequency range 150–850 cm^{-1}. The Raman spectrum of $SrTiO_3$ is dominated by two major scattering bands centered at 300 and 700 cm^{-1} in line with the literature (2, 3). The Raman spectrum of the other end member, $CaTiO_3$, also agrees with (16), where 9 Raman modes are observed at 155, 180, 226, 247, 286, 337, 471, 495, and 639 cm^{-1}. Actually, 117 vibrational modes ($3n - 3$) are expected for $CaTiO_3$ (C_{2V}^{14}; $Amm2$ and $Z = 8$), but most of these modes cannot be detected because of their low polarizabilities. Here, 8 Raman modes are observed at 175, 221, 244, 286, 336, 471, 492, and 677 cm^{-1}, in accordance with the positions in (16) except the highest frequency mode. The lower limit of our Raman scattering measurement cannot reveal the 155 cm^{-1} Raman band assigned to the Ca–TiO_3 lattice mode. An interesting feature is that the 460 cm^{-1} Raman band assigned to the Ti–O_3 torsional mode appears at $x = 0.6$, and that it shifts to the 471 cm^{-1} Raman mode of $CaTiO_3$ with x as demonstrated in Fig. 6. The upward shift of this Raman mode reflects the Ti–O bond distance and/or the Ti–O–Ti bond angle change between $SrTiO_3$ and $CaTiO_3$ (10).

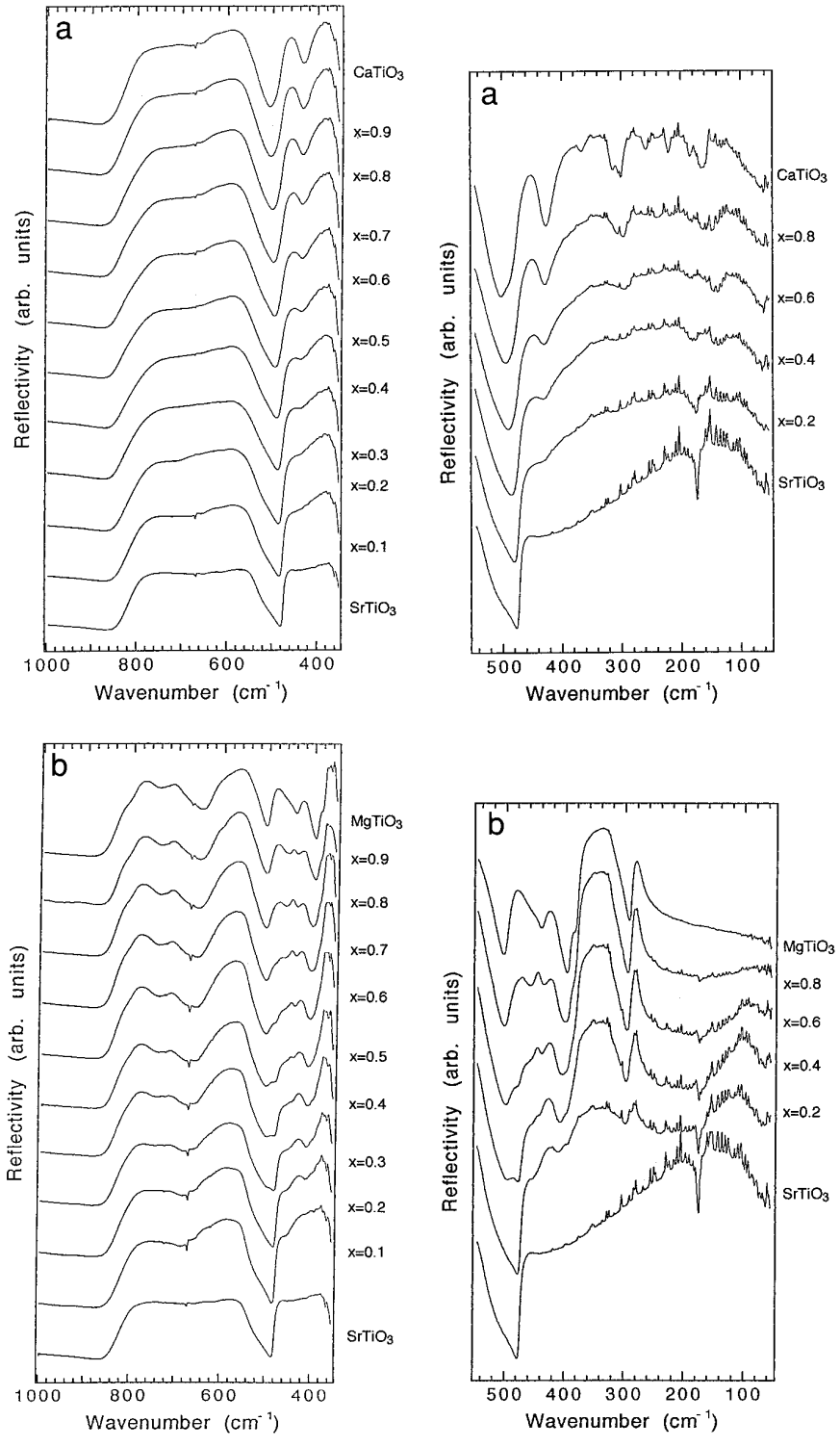

FIG. 4. The infrared-reflectivity spectra of $Sr_{1-x}Ca_xTiO_3$ (a) and $Sr_{1-x}Mg_xTiO_3$ (b) with different x's between 50–550 cm^{-1} and 350–1000 cm^{-1}, allowing for partial overlap.

Figure 5b shows the Raman spectra of $Sr_{1-x}Mg_xTiO_3$ with different x's. The Raman spectrum of $MgTiO_3$ ($R-3$: C_3i^2), in which the Raman-active modes $5A_g + 5E_g$ are predicted by the factor group analysis, is in good agreement with the literature (17, 22); all Raman-active modes are observed at 221, 281, 305, 327, 352, 398, 478, 501, 641, and 712 cm^{-1}; note that the 501 cm^{-1} mode is resolved as the shoulder. Some of these Raman modes would appear at

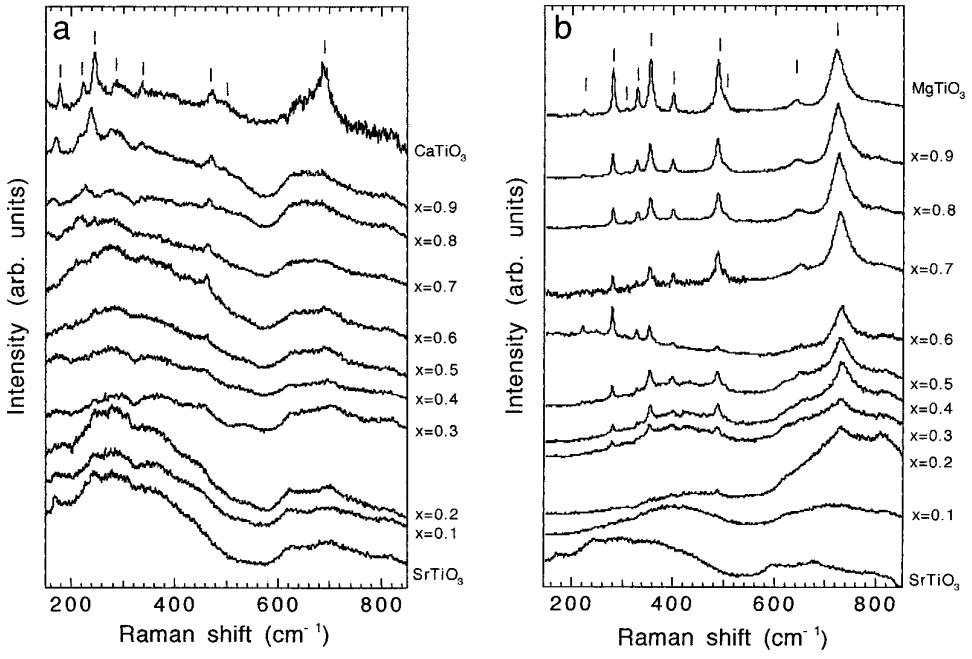

FIG. 5. The Raman spectra of $Sr_{1-x}Ca_xTiO_3$ (a) and $Sr_{1-x}Mg_xTiO_3$ (b) with different x's between 150 and 850 cm^{-1}.

$x \geq 0.3$ and increase in intensity with x in $Sr_{1-x}Mg_xTiO_3$. Particularly, the 712 cm^{-1} mode of $MgTiO_3$, which is assigned to the Ti–O stretching vibration of TiO_6 units (17, 22), appears at $x \geq 0.2$ and becomes sharp, increasing its intensity with x. This spectral change also implies that the formation of solid solutions is restricted to $x \leq 0.2$ for $Sr_{1-x}Mg_xTiO_3$.

4. DISCUSSION

The present work has revealed that the $Sr_{1-x}Ca_xTiO_3$ solid solutions are formed over a wide x range while traces of $CaTiO_3$ would appear for $x \geq 0.6$. On the other hand, the formation of the $Sr_{1-x}Mg_xTiO_3$ solid solutions is restricted to $x \leq 0.2$. All the techniques used in the present work could reach the same conclusion concerning the solubility of Ca or Mg in $SrTiO_3$. Now, we will address this issue in some detail. It has been found (23–25) that the enthalpy of formation of perovskite compounds, ΔH_f°, is well correlated with the tolerance factor t as defined in the Introduction; an empirical relation, $\Delta H_f^\circ = -125 + 1000(1 - t)$ in $kJmol^{-1}$, is established for $A^{II}B^{IV}O_3$ (23).

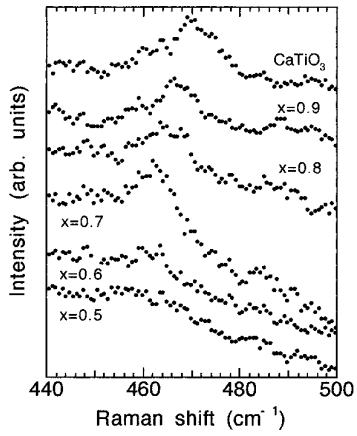

FIG. 6. The appearance of the 460 cm^{-1} Raman band at $x = 0.6$ and its upward shift with further increasing x in $Sr_{1-x}Ca_xTiO_3$.

Let the enthalpy of the reaction $(1 - x)SrTiO_3 + xCa(Mg)TiO_3 = Sr_{1-x}Ca(Mg)_xTiO_3$ be given by $(\Delta H_f^\circ)_{Ca}$ or $(\Delta H_f^\circ)_{Mg}$, respectively. Next, if assuming that $(\Delta H_f^\circ)_{Ca}$ or $(\Delta H_f^\circ)_{Mg}$ is described as the algebraic sum of the enthalpies of formation of $SrTiO_3$ and $CaTiO_3$ or $MgTiO_3$, the above empirical relation for $A^{II}B^{IV}O_3$ reduces to

$$(\Delta H_f^\circ)_{Ca} \text{ or } (\Delta H_f^\circ)_{Mg} = -125 + 1000[(1 - t) + x(t - t')],$$

where t and t' correspond to the tolerance factor of $SrTiO_3$, and $CaTiO_3$ or $MgTiO_3$. The validity of this equation is not confirmed because $(\Delta H_f^\circ)_{Ca}$ and $(\Delta H_f^\circ)_{Mg}$ are not determined experimentally for various x's. However, it tells us that the enthalpy of each reaction is predominated by the size of $(t - t')$ as well as x at $t \approx 1$. Interestingly enough, the second term dominates the enthalpy of reaction, such that $(t - t') > 0$ or $(t - t') < 0$ causes $(\Delta H_f^\circ)_{Ca}$ or $(\Delta H_f^\circ)_{Mg}$ to become less or more negative at $t \approx 1$. According to ion radii for the A or B cations with 12- or 6-coordination in ABO_3 (12) along with rO(II) = 1.21 Å and

$r_{Ti^{4+}}(VI) = 0.745$ Å, the tolerance factors are calculated to be 0.955, 0.922, and 0.810 for $SrTiO_3$, $CaTiO_3$, and $MgTiO_3$, respectively; the Mg^{2+} radius with 8-coordination was used in the calculation because of no available data for Mg^{2+} with 12-coordination.

With these tolerance factors, it follows that $Sr_{1-x}Mg_xTiO_3$ is less stable as compared with $Sr_{1-x}Ca_xTiO_3$. The difference $(t - t') = 0.148$ for $Sr_{1-x}Mg_xTiO_3$ is more influential on the enthalpy of reaction depending on x. The present thermodynamic argument accounts for the difficult synthesis of $Sr_{1-x}Mg_xTiO_3$ over a wide x range and the limited solubility of Mg in $SrTiO_3$ as well. In short, inefficient mixing of $MgTiO_3$ with $SrTiO_3$ is attributed to the substantial difference between the Sr^{2+} and Mg^{2+} cation radii, which leads to the less negative enthalpy of reaction through the tolerance factor limitations. Although it is generally agreed that the concentration of a solid solution is greatly restricted as the radius difference between two cations becomes large, it is a feature subject to establish if there is any correlation between tolerance factors and solubility limits of other cations in perovskites, by extending the present thermodynamic argument.

For the $SrTiO_3$–$CaTiO_3$ system, the similar ionic size between the Sr^{2+} and Ca^{2+} cations would facilitate the formation of the $Sr_{1-x}Ca_xTiO_3$ solid solutions over a wide x range. Meanwhile, it is of particular interest that the Sr–O bond length reduction is somewhat matched by the Ti–O bond shortening upon Ca^{2+} substitution. This is evidenced by the fact that the 460 cm^{-1} Raman band assigned to the Ti–O_3 torsional mode appears at $x = 0.6$ and shifts upward with further increasing x. The smaller Ca^{2+} interacts with anions more strongly, and thereby distorts the TiO_6 octahedron so as to give the resultant upward shift of the Raman mode in question.

Finally, sol–gel processes or synthesis at high pressures/temperatures may expand the solubility range for the $Sr_{1-x}Mg_xTiO_3$ solid solutions. However, we stress that our essential part of the argument remains ineffective.

5. CONCLUSIONS

The perovskite compounds $Sr_{1-x}M_xTiO_3$ (M = Ca; Mg) have been synthesized by solid-state reaction, and characterized by Fourier-transform infrared spectroscopy, Raman scattering, and X-ray diffraction. It was found that the $Sr_{1-x}Ca_xTiO_3$ solid solutions are formed over a wide x range while traces of $CaTiO_3$ appear for $x \ge 0.6$. On the other hand, the formation of the $Sr_{1-x}Mg_xTiO_3$ solid solutions is restricted to $x \le 0.2$. The solubility of Ca or Mg in $SrTiO_3$ is discussed based on the correlation between the enthalpy and tolerance factors for $A^{II}B^{IV}O_3$. It is concluded that the more limited solubility of Mg in $SrTiO_3$ is attributed to the substantial difference between the Sr^{2+} and Mg^{2+} cation radii, which leads to less stable $Sr_{1-x}Mg_xTiO_3$ through a significant contribution due to the tolerance factor difference between $SrTiO_3$ and $MgTiO_3$ as compared with $CaTiO_3$. The present argument also accounts for the formation of the $Sr_{1-x}Ca_xTiO_3$ solid solutions over a wide x range, because of their similar size between Sr^{2+} and Ca^{2+}. For the $SrTiO_3$–$CaTiO_3$ system, it is of interest that the Sr–O bond length reduction is somewhat matched by the Ti–O bond shortening upon Ca^{2+} substitution. This is evidenced by the fact that the 460 cm^{-1} Raman band assigned to the Ti–O_3 torsional mode appears at $x = 0.6$, and shifts upward with further increasing x.

ACKNOWLEDGMENT

We are indebted to H. Doi for X-ray diffraction of the perovskite compounds prepared in the present work.

REFERENCES

1. G. Shirane and Y. Yamada, *Phys. Rev.* **177,** 858 (1969).
2. U. Bianchi, W. Kleemann, and J. G. Bednorz, *J. Phys.: Condens. Matter* **6,** 1229 (1994).
3. J. Meng, G. Zou, Y. Ma, X. Wang, and M. Zhao, *J. Phys.: Condens. Matter* **6,** 6549 (1994).
4. J. L. Brebner, S. Jandl, and Y. Lepine, *Phys. Rev. B* **23,** 3816 (1981).
5. A. F. W. Klukhuhn, J. Bruining, B. Klootwijk, and J. v. d. Elsken, *Phys. Rev. Lett.* **25,** 380 (1970).
6. A. Reller, *Phil. Mag. A* **68,** 641 (1993).
7. S. L. Cuffini, V. A. Macagno, R. E. Carbonio, A. Melo, E. Trollund, and J. L. Gautier, *J. Solid State Chem.* **105,** 161 (1993).
8. V. M. Goldschmidt, *Strifter Nordske Videnskaps-Akad. Oslo, 1. Mat,-Naturv. K1.,* **8,** 2 (1926).
9. C. Eylem, H. L. Ju, B. W. Eichhorn, and R. L. Greene, *J. Solid State Chem.* **114,** 164 (1995).
10. H. L. Ju, C. Eylem, J. L. Peng, B. W. Eichhorn, and R. L. Greene, *Phys. Rev. B* **49,** 13335 (1994).
11. J. E. Sunstrom, IV, S. M. Kauzlarich, and M. R. Antonio, *Chem. Mater.* **5,** 182 (1993).
12. R. D. Shannon, *Acta Crystallogr. Sect. A* **32,** 751 (1976).
13. M. Ceh, D. Kolar and L. Golic, *J. Solid State Chem.* **68,** 68 (1987).
14. Y. Kawada and M. Fujimoto, *Jpn. J. Appl. Phys.* **29,** L126 (1990).
15. C. H. Perry, B. N. Khanna, and G. Rupprecht, *Phys. Rev. A* **135,** 408 (1964).
16. U. Balachandran and N. G. Eror, *Solid State Commun.* **44,** 815 (1982).
17. B. Reynard and F. Guyot, *Phys. Chem. Miner.* **21,** 441 (1994).
18. B. A. Wechsler and R. B. Von Dreele, *Acta Crystallogr. Sect. B* **45,** 542 (1989).
19. C. H. Perry, D. J. McCarthy, and G. Rupprecht, *Phys. Rev. A* **138,** 1537 (1965).
20. W. G. Spitzer, R. C. Miller, D. A. Kleinman, and L. E. Howarth, *Phys. Rev.* **126,** 1710 (1962).
21. V. M. Ferreira, J. L. Baptista, S. Kamba, and J. Petzelt, *J. Mater. Sci.* **28,** 5894 (1993).
22. N. L. Ross and P. McMillan, *Am. Mineral.* **65,** 719 (1984).
23. H. Yokokawa, T. Kawada, and M. Dokiya, *J. Am. Ceram. Soc.* **72,** 152 (1989).
24. E. Takayama-Muromachi and A. Navrotsky, *J. Solid State Chem.* **72,** 244 (1988).
25. H. Yokokawa, N. Sakai, T. Kawada, and M. Dokiya, *J. Solid State Chem.* **94,** 106 (1991).